Journal of Power Sources 221 (2013) 149–156

Contents lists available at SciVerse ScienceDirect

Journal of Power Sources

journal homepage: www.elsevier.com/locate/jpowsour

Ba-substituted LSCM anodes for solid oxide fuel cells

E. Lay [a,b,*], L. Dessemond [a], G. Gauthier [b,1]

[a] LEPMI, Laboratoire d'Electrochimie et de Physico-chimie des Matériaux et des Interfaces, UMR 5279, CNRS – Grenoble INP – Université de Savoie – Université Joseph Fourier, 1130 rue de la piscine, BP 75, 38402 Saint Martin d'Hères, France
[b] CEA, LITEN, DEHT, F-38054 Grenoble, France

HIGHLIGHTS

- Barium was substituted for Strontium in the mixed conducting perovskite oxide LSCM.
- In CO_2-free gases, materials are stable in SOFC anodic conditions.
- Barium substitution improves the electrical p-type semi-conductivity in argon.
- In H_2–H_2O the conductivity varies between 0.5 and 0.9 S cm^{-1} at 900 °C.
- Electrochemical performances are interesting for applicability as an SOFC anode material.

ARTICLE INFO

Article history:
Received 10 April 2012
Received in revised form
23 July 2012
Accepted 31 July 2012
Available online 13 August 2012

Keywords:
SOFC
Anode
Barium
LSCM

ABSTRACT

Three perovskites with the general formula $La_{0.75}Ba_xSr_{0.25-x}Cr_{0.5}Mn_{0.5}O_3$ ($x = 0$, 0.10 and 0.25) have been synthesized. For all materials, the symmetry is rhombohedral (space group R-3c). On the electrical point of view, a p-type semiconducting behaviour was evidenced in the series. The addition of barium yields an increase in total conductivity in argon from 18 S cm^{-1} for $La_{0.75}Sr_{0.25}Cr_{0.5}Mn_{0.5}O_3$ to 26 S cm^{-1} for $La_{0.75}Ba_{0.25}Cr_{0.5}Mn_{0.5}O_3$ at 900 °C. However, in H_2–3% H_2O, the total conductivity decreases for all compositions and it decreases with barium substitution (0.9 S cm^{-1} for $La_{0.75}Sr_{0.25}Cr_{0.5}Mn_{0.5}O_3$ and 0.5 S cm^{-1} for $La_{0.75}Ba_{0.25}Cr_{0.5}Mn_{0.5}O_3$ at 900 °C). Steady state and impedance spectroscopy measurements were performed on dense pin-shaped electrodes ($x = 0$ and 0.25) in H_2–3% H_2O between 800 and 900 °C. For $x = 0.25$, electrochemical performances are interesting for an applicability as an SOFC anode. Origins of individual contributions to the electrode reaction mechanism are discussed.

© 2012 Elsevier B.V. All rights reserved.

1. Introduction

Ni–YSZ cermet is the usual anode material for zirconia-based solid oxide fuel cells (SOFCs). In spite of excellent electrocatalytic properties for fuel oxidation and good current collection, Ni–YSZ suffers some drawbacks, such as carbon deposition under hydrocarbon feed and poor redox cycling [1]. Different approaches exist to overcome the low durability, such as searching for alternative materials for anode. In this scope, the development of mixed-conducting perovskite oxides, *e.g.* substituted strontium titanates or lanthanum chromites, has recently received great attention [2,3]. The lanthanum and strontium chromo-manganite $La_{0.75}Sr_{0.25}Cr_{0.5}Mn_{0.5}O_{3-\delta}$ (LSCM) was reported to be a promising anode material to replace Ni–YSZ cermets, demonstrating both good performances as a catalytic material for H_2 and CH_4 oxidation and redox stability in low steam to hydrocarbon ratios [2]. Nevertheless, LSCM presents a low conductivity in air and in reducing conditions [4], and oxygen diffusion as well as surface exchange properties of LSCM [5] are lower than in other perovskites [6]. Although LSCM represents a promising anode material for SOFCs [7], various studies have been performed on LSCM based composites with yttria stabilized zirconia [8], gadolinia doped ceria [9] or with metal catalysts [10,11] to improve the anodic performance. The effects of the content and/or the nature of the dopant at A- or B-sites of $La_{1-x}Sr_xCr_{1-y}Mn_yO_{3-\delta}$ solid solutions on electric and electrocatalytic properties have been also evaluated [12–16] to assess the potential of these oxides as SOFC anodes. For instance, 10% of cerium substituted on the A-sites of LSCM was found to enhance electrochemical performance without additional microstructural modification and without any change of the electrical conductivity in a reducing atmosphere [17]. Using the chemical flexibility of the perovskite structure, barium was partially or totally substituted for strontium in LSCM, in order to study the effect of the material

* Corresponding author. CEA, LITEN, DEHT, 17 rue des Martyrs, 38054 Grenoble, France. Tel.: +33 (0) 438784274; fax: +33 (0) 438785198.
E-mail addresses: elisa.lay@grenoble-inp.org, elisa.lay@cea.fr (E. Lay).
[1] Presently Professor at the Universidad Industrial de Santander, Bucaramanga, Colombia.

0378-7753/$ – see front matter © 2012 Elsevier B.V. All rights reserved.
http://dx.doi.org/10.1016/j.jpowsour.2012.07.126

basicity on its overall performance. The generally higher basicity of barium oxides can play an interesting role in H_2 oxidation [18] or in decoking reactions in case of complex organic fuels [19–21]. Indeed, in Solid Oxide Fuel Cells, the anode atmosphere may contain a high concentration of CO_2 when operating on carbon-containing fuel whereas the cathode atmosphere typically contains a low level of CO_2. Although stability problems in atmospheres containing water and carbon dioxide are generally suspected for barium containing oxides [22,23], CO_2 and H_2O sensibility could be actually an advantage to avoid anode coking, as recently shown in the case of Ba-modified cermets [24].

To our knowledge, the effect of barium at the A-site of lanthanum chromo-manganite on the electrochemical activity for the hydrogen oxidation has been only studied by Zhang et al. [25]. Unfortunately, the reported results are not so convincing since the formation of a secondary phase has been evidenced.

In this first work, structural properties, stability, electrical properties and SOFC anodic behaviour have been compared within the $La_{0.75}Ba_xSr_{0.25-x}Cr_{0.5}Mn_{0.5}O_3$ series in the absence of CO_2, the influence of carbon dioxide being considered in a forthcoming study. The electrochemical oxidation mechanism in wet hydrogen is also discussed.

2. Experimental

2.1. Synthesis

Powders of $La_{0.75}Sr_{0.25}Cr_{0.5}Mn_{0.5}O_3$ and $La_{0.75}Ba_xSr_{0.25-x}Cr_{0.5}Mn_{0.5}O_3$ ($x = 0.1, 0.25$) were synthesized by a citrate nitrate route, well described in literature ([26] and references therein). The samples will be referenced as LSCM, LBSCM and LBCM, respectively. The exact conditions of synthesis are described into details elsewhere [27], using the following precursors: $SrCO_3$ (Alfa Aesar, 99.9%), $MnCO_3$ (Alfa Aesar, 99.985%), $BaCO_3$ (Alfa Aesar, 99.95%) and $Cr(NO_3)_3.9H_2O$ (Alfa Aesar, 99.99%). The heat treatment of Ba containing powders was carried out in argon in order to avoid the formation of barium chromate and barium manganate. LSCM was also synthesized in argon for a comparison purpose. Phase purity was checked by X-ray diffraction (XRD) at room temperature using a Bruker AXS D8 Advance diffractometer working in vertical Bragg-Brentano geometry and equipped with a Cu anticathode ($K\alpha_{1,2}$ radiations), a backside graphite monochromator and a scintillation detector used in the range $2\theta = 10–110°$, with 0.02° and 10 s of angular and time steps, respectively. The Fullprof Suite software [28] was used for Rietveld refinements, using a Pseudo-Voigt function for the peak profiles: the non-special atomic positions as well as the isotropic atomic displacements of all atom groups were refined. When several atoms shared the same atomic site, a statistic occupation was considered. Estimated standard deviations were systematically corrected with Berar and Lelann σ_{corr} factor [29].

After a firing step at 1100 °C for 2 h in argon, the as-obtained powders were ground, compacted at 0.2 MPa and isostatically pressed at 300 MPa. Dense pellets (>93% of the theoretical density) of single phase materials were processed by sintering the green samples at 1500 °C for 10 h in argon.

2.2. Chemical stability

Chemical stability was examined in operating conditions before performing electrical and electrochemical characterizations. Experiments have been carried out in a large panel of CO_2-free atmospheres in order to cover a large range of oxygen partial pressures corresponding to working conditions not only of an SOFC anode but also of an Solid Oxide Electrolysis Cell (SOEC) cathode, as both applications are not so different. For such purposes, powders were heated at 900 °C for 48 h in wet (20% H_2O) H_2–Ar (SOEC cathode), dry H_2–Ar (extreme conditions for SOFC anode), air (SOFC cathode/SOEC anode). Wet atmosphere (20% H_2O) was obtained by gas bubbling through deionised water at 60 °C.

2.3. Electrical measurements

Dense pellets of LSCM, LBSCM and LBCM samples were machined with diamond tools to a cylindrical shape of around 10 mm in height and 6 mm in diameter, with two grooves of 1 mm depth. Using the four point probe dc technique, the thermal evolution of electrical conductivity was recorded in dry argon and wet (3% H_2O) hydrogen for temperature up to 900 °C during one thermal cycle. Wet hydrogen was obtained by gas bubbling through deionised water at room temperature. The gas flow rate was 10 mL min^{-1}. Platinum paste (Metalor, No. 6982) was painted on both ends of the sample as current probes. Current collection was ensured by using platinum grids and wires (Fig. 1). The potential probes consisted in platinum wires (0.2 mm in diameter) inserted into the grooves, and maintained with platinum paste. The samples were heated at 800 °C to sinter the conducting paste. Conductivity measurements were performed for current from 0.1 to 100 mA, using a Tacussel potentiostat (PGS201T) and then measuring the voltage drop across the two middle wires (Hewlett Packard 34401A multimeter). The corresponding resistance was calculated by applying the classical Ohm's law. Conductivity values were then deduced from the resistance data considering the appropriate geometrical factor. For a better comparison, electrical conductivities were corrected by taking into account the sample density [30].

2.4. Electrochemical characterization

Steady state and impedance spectroscopy measurements have been performed on dense pin-shaped LSCM and LBCM electrodes in order to avoid any effect of the electrode microstructure on the recorded responses. The electrolyte pellet was prepared from a YSZ commercial powder containing 8 mol% Y_2O_3 (TZ8Y from Tosoh, sintered at 1500 °C for 2 h). The working electrodes were machined

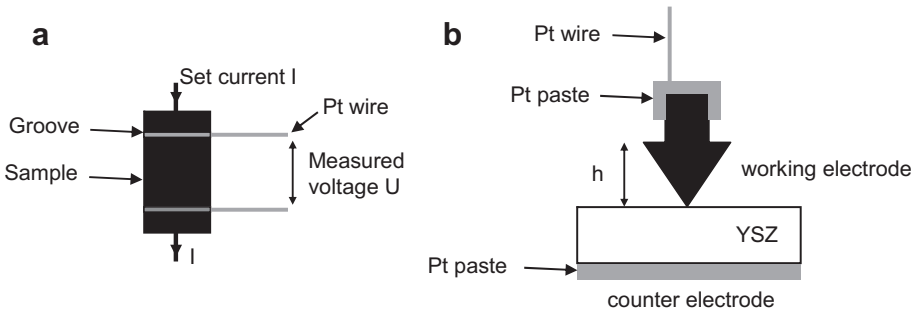

Fig. 1. Schemes of (a) electrical and (b) electrochemical measurement cells.

with diamond tools (4 mm in height and 4 mm in diameter on their flat bases). Experiments were carried out between 800 and 900 °C in wet H_2 (3% H_2O). The gas flow rate was chosen equal to 100 mL min^{-1}. The counter electrode was painted using a platinum paste (Metalor) on the opposite side of the YSZ pellet, and platinum wires were used as current collectors. Current collection in anodes was ensured by depositing platinum paste on the top of pin-shaped electrodes (Fig. 1). High frequency impedance diagrams were recorded first at open circuit potential (OCP) using a Hewlett–Packard impedancemeter (HP 4192 A LF) between 5 and 1.3×10^7 Hz in order to characterize the contact between electrodes and YSZ. The amplitude of the measuring signal was 50 mV to obtain well-defined diagrams. The low frequency electrode characteristics at OCP and for anodic potentials were recorded using an Autolab potensiostat equipped with an impedance frequency analyzer (Eco-Chemie, The Netherlands) in the frequency range 10^{-3}–10^4 Hz. The amplitude of the measuring signal was varied between 10 and 50 mV to ensure the linearity of the impedance response. For the sake of comparison, the series resistance determined from the high frequency intercept of the electrode impedance on the real axis in the Nyquist plane, and which represents the sum of the electrolyte resistance and additional contacts, has been subtracted. The numbers on impedance diagrams indicate the logarithm of the measuring frequency. Cyclic voltammetry measurements were performed for anodic potentials up to 0.65 V (sweep rate: 1 mV s^{-1}). Impedance measurements under current were performed after waiting at least 120 s till the steady-state current was reached.

3. Results

3.1. Structural analysis

The room temperature XRD powder patterns of $La_{0.75}Sr_{0.25}Cr_{0.5}Mn_{0.5}O_{3-\delta}$ (LSCM) and $La_{0.75}Ba_xSr_{0.25-x}Cr_{0.5}Mn_{0.5}O_{3-\delta}$ with $x = 0.10$ and 0.25 (LSBCM and LBCM) fired at 1500 °C in argon are shown in Fig. 2. For every compositions, the peak indexation confirms a rhombohedral perovskite structure (S.G. $R\bar{3}c$, No. 167), as already observed for LSCM in the literature [2,17]. The structural parameters obtained from Rietveld refinements using those diffraction data are summarized in Table 1.

Results of Table 1 show a global increase in cell parameters with barium substitution. This trend is in agreement with a Ba^{2+} ionic radius in 12-fold coordination, markedly larger than for Sr^{2+} (161 pm vs. 144 pm, respectively [31]).

3.2. Chemical stability

At the detection level of the technique, Ba doped materials are regarded as stable at 900 °C whatever the atmosphere, since there is no additional Bragg peak in their respective XRD patterns (Fig. 3), even if a $BaCr_2O_4$ phase might be considered [32]. XRD patterns of LSCM after the same tests are also presented for comparison.

Substitution by barium is shown to improve the perovskite stability in reducing atmospheres since the decomposition into a Ruddlesden Popper type chromo-manganite, evidenced for LSCM in dry H_2, does not occur for Ba-doped LSCM materials. Indeed, as can be seen, LSCM is stable in wet H_2 (2% H_2–3% H_2O–Ar) but not in dry H_2 as a $(La,Sr)_2MnO_4$ type phase is formed. Ruddlesden Popper phases are thermodynamically more stable than perovskite ones in a reducing environment because of the lower valence state of manganese than in the parent perovskite structure. Depending on lanthanum content, and especially for the La-rich part of the family,

Table 1
Room-temperature structural parameters obtained from X-ray powder diffraction data of LSCM, LSBCM and LBCM samples prepared in argon. Reliability factors of Rietveld refinement are specified. B_{iso} values were fixed as follow: $B_{iso} = 0.8$, 0.6 and 1.2 $Å^2$ for A-site cations, B-site cations and oxygen, respectively.

Composition	LSCM	LSBCM	LBCM
Space group	$R\bar{3}c$(167)	$R\bar{3}c$(167)	$R\bar{3}c$(167)
a Å	5.5031(1)	5.5124(1)	5.5236(4)
c Å	13.3448(4)	13.4013(5)	13.466(1)
V $Å^3$	349.99(2)	352.66(2)	355.83(6)
Z	6	6	6
Oxygen position x	0.453(4)	0.458(2)	0.468(6)
χ^2	1.55	1.35	2.00
R_p/%, R_{wp}/%, R_{Bragg}	10.4, 13.6, 13.9	20.4, 21.7, 18.18	11.8, 15.5, 10.93

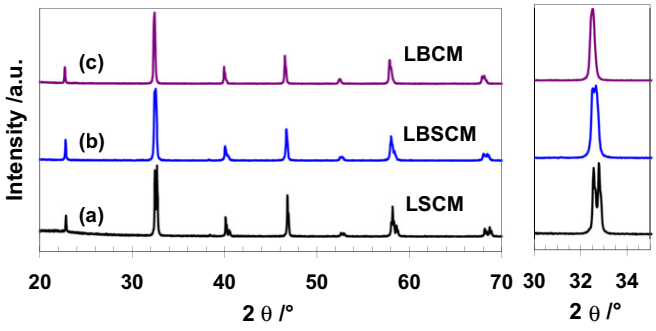

Fig. 2. XRD powder diffraction patterns of (a) LSCM, (b) LSBCM and (c) LBCM prepared at 1500 °C in argon.

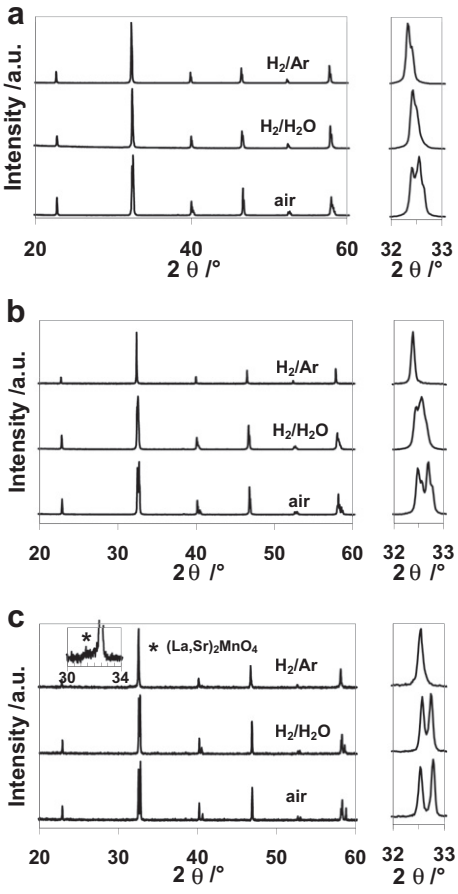

Fig. 3. XRD powder diffraction patterns of (a) LBCM and (b) LSBCM after stability tests in air, 2% H_2–20% H_2O–Ar and 2% H_2–Ar and (c) LSCM after stability tests in air, 2% H_2–3% H_2O–Ar and 2% H_2–Ar.

LSM generally decomposes in reducing conditions at high temperature into $(La,Sr)_2MnO_4$ and MnO [33]. Even if chromium is substituted for manganese in LSCM for stability reasons, a partial decomposition into $(La,Sr)_2(Cr,Mn)O_4$ after firing in pure H_2 for 5 h at 1000 °C was already reported by Fonseca et al. [15], in agreement with this study. Thus, only Eq. (1) is likely to occur instead of a more complete decomposition because of the partial stabilization with chromium:

$$2AMn^{+III/+IV}O_3 \rightarrow A_2Mn^{+II/+III}O_4 + Mn^{+II}O + 1/2\,O_2 \quad (1)$$

with A = (La,Sr) and Cr probably doping the Mn site of the Ruddlesden Popper phase.

LSCM, LSBCM and LBCM structures remain rhombohedral in air and in 2% H_2–20% H_2O–Ar (atmosphere referred as H_2/H_2O). Structure parameters were hence refined in the same respective space group as after synthesis in argon. On the contrary, LBCM and LSBCM structures become cubic in dry H_2 (atmosphere referenced as H_2/Ar). The improvement in symmetry compared to LSCM structure, could explain the phase stabilization. These results indicate that Ba-doped LSCM should be stable in normal SOFC anode operating conditions (H_2–H_2O–(Ar) mixing).

Lattice parameters were refined in order to compare their trends in function of oxygen partial pressure (Table 2). Cell parameters present a slight linear increase while oxygen partial pressure decreases. This expansion is likely linked to the reduction of manganese and chromium valence states from (+3)/(+4) to (+3) [34]. Indeed, Mn^{4+} and Mn^{3+} radii are equal to 53 and 64.5 pm, respectively, and Cr^{4+} and Cr^{3+} radii are equal to 41 and 61.5 pm, respectively ($Z = 6$) [31]. Besides, the reduction of manganese and chromium valence states results in oxygen vacancy formation according to:

$$2M_M^{\bullet} + O_O^{\times} = 2M_M^{\times} + V_O^{\bullet\bullet} + 1/2\,O_2 \quad (2)$$

The induced increase of repulsion between second neighbouring cations could also explain this expansion.

3.3. Electrical conductivity

Since the thermochemical stability of LSCM, LBSCM and LBCM has been proved in a reducing atmosphere (Fig. 3), the conduction behaviour has been investigated in argon and wet hydrogen (3% H_2O). Accordingly, the variations of total conductivity versus temperature and oxygen partial pressure cannot be related to any impurity phase formation in the chosen experimental conditions. This was confirmed by the absence of any thermal hysteresis. The temperature dependences of the total conductivity for the three oxides are shown in Fig. 4. Between 350 and 900 °C, a typical Arrhenius behaviour was assumed for all conditions. The corresponding activation energies as well as the conductivity values determined at 900 °C are reported in Table 3. They are close to those reported for the p-type semi-conducting LSCM [2,19].

The conduction mechanisms are certainly similar in all those chromo-manganites materials, mainly driven by the presence of Mn at the B-site of the perovskite [34]. The thermal activation of conductivity with temperature and the conductivity values indicate that these oxides are semi-conductors in the whole examined temperature range. A p-type semi-conductivity, related to Mn in the 4+ and 3+ oxidation states, is brought out by the decrease in conductivity at lower oxygen partial pressures. For instance, total conductivities at 900 °C of LBSCM in argon and wet hydrogen are 24.43 and 0.52 S cm^{-1}, respectively. For LBCM they are 25.96 and 0.52 S cm^{-1}, respectively. The activation energies (Table 3) are in the 0.24–0.63 eV range. These values are typical for a small polaron mechanism between Mn^{3+} and Mn^{4+} localized states and in particular in chromo-manganites [35–37].

In argon, the substitution of barium for strontium results in an increase in conductivity (Fig. 4(a)). Barium and strontium having the same oxidation state (+2), no modification of manganese oxidation state can be thus expected by replacing strontium by barium. As a consequence, the observed increase in conductivity seems to be related to an increase in charge carrier mobility. Indeed, the conductivity does not depend only on the number of Mn^{3+}–Mn^{4+} pairs but also on the crystal structure. A larger overlap between O-2p and Mn-3d orbitals enhances the charge carrier exchange and is expected to be optimal when the Mn–O–Mn angle is close to 180° and/or the Mn–O bond length is small [38]. The Mn–O–Mn angles obtained by Rietveld refinements are 165.080°, 166.497° and 169.776°, respectively, for LSCM, LSBCM and LBCM. The overlap between O-2p and Mn-3d orbitals is apparently improved with barium addition, leading to a higher mobility of charge carriers.

In wet hydrogen, the total conductivity decreases for all compositions. At low oxygen partial pressures, charge compensation is achieved by oxygen vacancies formation (Eq. (2)). This implies that the whole concentration decreases in reducing conditions (p-type behaviour). Thus, the reduction of the material below a certain level must also yield an increasing oxygen deficiency [34]. The more pronounced slope of the Arrhenius curve indicates that the corresponding activation energy increases, in agreement with literature data on LSCM ceramics [4]. As confirmed by XRD analyses in reducing conditions (Fig. 3), the lattice expansion due to the reduction of transition elements at B-sites [4] also increases the Mn–O bond length, probably inhibiting the transport of charge carriers [2]. Differences of conductivity observed between LSCM and Ba-doped LSCM samples are reduced. Oxidation states of Cr and Mn are certainly similar, whatever the composition. The conduction mechanism appears identical, which suggests that charge carrier concentrations must be similar in those conditions.

The low conductivity values recorded in wet hydrogen are near the minimum value initially proposed for an anode material, which could be a disadvantage as compared to a Ni–YSZ cermet [39]. Nevertheless, quite recently, such value has been re-examined [40], considering that an effective electrode structure could consist of two different layers optimized for their respective function: the

Table 2
Room-temperature structural parameters obtained from X-ray powder diffraction data of LSCM, LSBCM and LBCM samples after a stability test. V_{eq} is the volume equivalent expressed with the same number of formula unit per cell ($Z = 1$).

Composition	LSCM			LSBCM			LBCM		
Atmosphere	Air	H_2/H_2O	H_2/Ar	Air	H_2/H_2O	H_2/Ar	Air	H_2/H_2O	H_2/Ar
Space group	R-3c	R-3c	Unstable	R-3c	R-3c	Pm-3m	R-3c	R-3c	Pm-3m
a Å[1]	5.49,867(5)	5.5058(1)	–	5.5075(1)	5.5155(1)	3.90,508(8)	5.5212(2)	5.5297(3)	3.9160(2)
c Å[1]	13.3184(2)	13.3813(4)	–	13.3669(3)	13.4287(4)	3.90,508(8)	13.4356(4)	13.542(2)	3.9160(2)
V Å^3	348.737(7)	351.30(2)	–	351.13(1)	353.79(2)	59.551(1)	354.70(2)	358.61(7)	60.053(5)
Z	6	6	–	6	6	1	6	6	1
V_{eq} Å^3	58.122(1)	58.550(3)	–	58.522(2)	58.96(3)	59.551(1)	59.12(1)	59.77(1)	60.053(5)

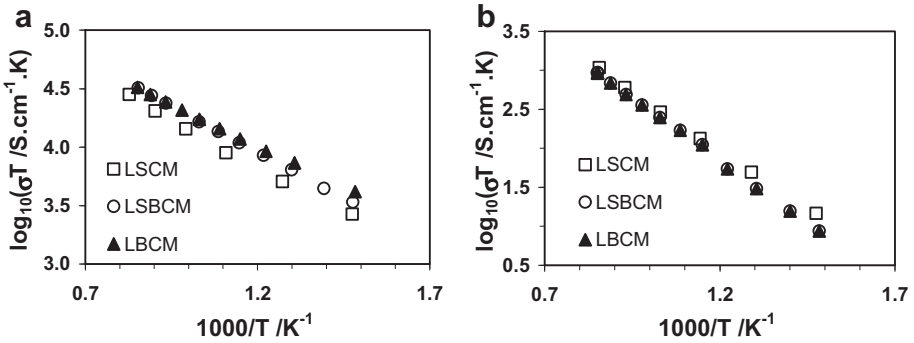

Fig. 4. Electrical conductivities in (a) argon and (b) H_2–3% H_2O.

electrochemical reaction in a thin functional layer in contact with the electrolyte substrate, and the upper layer acting as a current collector. The former layer should be optimized to display a good electrocatalytic activity and the latter to exhibit the lower electrical resistance. For a sufficiently thin layer (*i.e.* thickness lower than 10 μm), the total conductivity in the active layer could be as low as 10^{-2} S cm^{-1}. Accordingly, barium containing LSCM ceramics can meet this criterion.

3.4. Electrochemical characterization of LBCM and LSCM

In order to compare experimental data, normalized polarization resistances and current densities are used. By assuming that the contact zone between electrode and electrolyte is a disk, the contact area was calculated applying Newman's formula [41]. Effective area radii around 20 and 30 μm were determined for LBCM and LSCM, respectively. Contact areas were regularly checked during experiments.

Before stating on the influence of Ba substitution on the electrochemical properties of LSCM electrodes, one must clarify how much platinum, used as current collector in this study, contribute to the overall anode performance. Indeed, Pt can be regarded as catalytically active for the oxidation of H_2, in comparison with other noble metals like silver or gold [42]. Platinum current collector (mesh, paste or sputtering) has been widely used for studying the performance of porous LSCM based anodes [43–50]. But, there is some controversy in the literature on the effect of Pt on the anode polarization [51–53]. Although sputtering of platinum was not thought to help the oxidation of H_2 by LSCM [54], a recent report indicate that Pt should not be used for current collection when testing ceramic anodes [55]. Regardless of the electrode microstructure, the location of metal atoms is critical since the catalytic metal must be located near the triple phase boundary (TPB) sites in order to promote the oxidation of oxygen anions coming from the electrolyte. Because the ionic conductivity of LSCM is low [34], the TPB sites would not be optimized by a simple metal coating. Moreover, the active sites for oxidation are restrained to the proximity of the electrode/electrolyte interface when the electronic conductivity prevails [56].

One way to estimate the geometric extension of the reaction zone is to calculate the specific length L_D [57] which indicates that an interface process is dominating for thicknesses lower than L_D and that bulk diffusion is a limiting process for higher values. From exchange and diffusion properties of LSCM [5], one can estimate that L_D is of the order of 1 mm at 900 °C in a H_2 atmosphere. For porous electrodes of thickness lower than 100 μm, one can thus anticipate that the use of Pt for current collecting could influence the performance of the electrode, assuming that the whole volume of the electrode is active. Let us add that the migration of metal atoms within the porous electrode could magnify the related effect [55], as observed for impregnated anodes [51].

For thick and dense electrodes, the situation is markedly different. Considering the influence of the oxygen ions flux in LSCM on the related anode behaviour [12,14], the re-oxidation of active sites is likely to occur by bulk ion transport in the perovskite phase, as clearly evidenced for a thin (~0.5 μm thick) and dense LSCM film [58]. Since the platinum paste and wires are located 4–5 mm away from the electrode/electrolyte interface (Fig. 1), and as the conductivity of oxides is rather low (Fig. 4), metal atoms cannot be regarded as active sites for the oxidation of H_2 in the chosen experimental conditions. Accordingly, one can assume that the recorded variations are not related to any contribution of platinum. This also allows to normalize current, resistance and capacitance values by the contact area between pin-shaped electrodes and YSZ.

In the chosen experimental conditions, two elementary contributions can be separated at high and low frequencies in the electrode characteristics (Fig. 5) and are thus referenced as HF and LF. The sum of corresponding resistances R_{HF} and R_{LF} represents the polarization resistance R_{pol}. This agrees with previous reports on LSCM based anodes in humidified hydrogen [43,44,58]. As shown in Fig. 6, all resistances are thermally activated and the corresponding activation energies are reported in Table 4. For the LSCM anode, the polarization resistance R_{pol} is equal to 27.1 Ω cm^2 at 800 °C and to 7.6 Ω cm^2 at 900 °C. These values are higher than those reported in the literature for porous electrodes [2,59], as could be expected for dense electrodes [39]. The activation energy is higher than that determined by Ruiz-Morales et al. (0.84 eV between 850 and 950 °C in H_2–5% H_2O) [46], but it is closed to those reported for H_2 oxidation on $La_{0.8}Sr_{0.2}Cr_{0.97}V_{0.03}O_3$ (between 1.66 and 2.08 eV) [60]. It is evident that the oxidation reaction on LSCM is dominated by the LF process since its magnitude represents around 80% of the polarization resistance. The substitution of strontium by barium in the A-sites of the perovskite yields a decrease of R_{pol} (Fig. 6). Indeed, R_{pol} is equal to 17.2 and 3.3 Ω cm^2 at respectively 800 and 900 °C. This is accompanied by a marked decrease of the LF resistance since its magnitude represents nearly

Table 3
Activation energies and conductivity values at 900 °C.

Composition		Argon	H_2–3% H_2O
$La_{0.75}Ba_{0.25}Cr_{0.5}Mn_{0.5}O_3$	Ea eV	0.24	0.63
	σ(900 °C) S cm^{-1}	25.96	0.52
$La_{0.75}Ba_{0.1}Sr_{0.15}Cr_{0.5}Mn_{0.5}O_3$	Ea eV	0.32	0.54
	σ(900 °C) S cm^{-1}	24.43	0.52
$La_{0.75}Sr_{0.25}Cr_{0.5}Mn_{0.5}O_3$	Ea eV	0.28	0.54
	σ(900 °C) S cm^{-1}	18.3	0.9

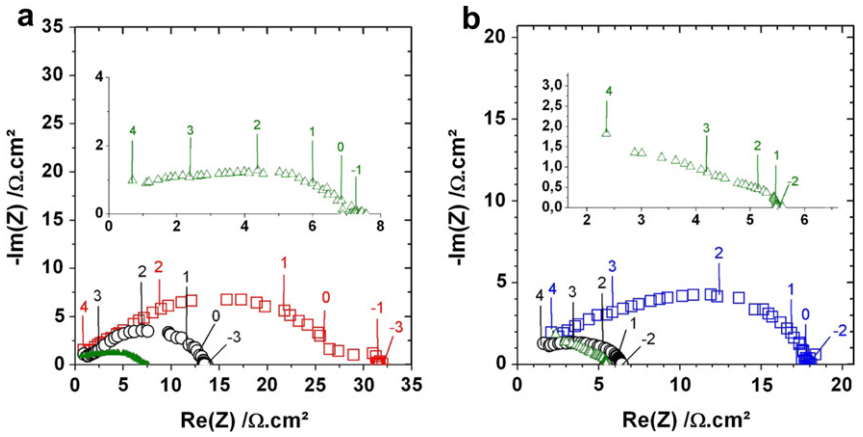

Fig. 5. Electrode characteristics recorded at OCP on (a) LSCM and (b) LBCM in H_2–3% H_2O at (□) 800 °C, (○) 850 °C and (Δ) 900 °C.

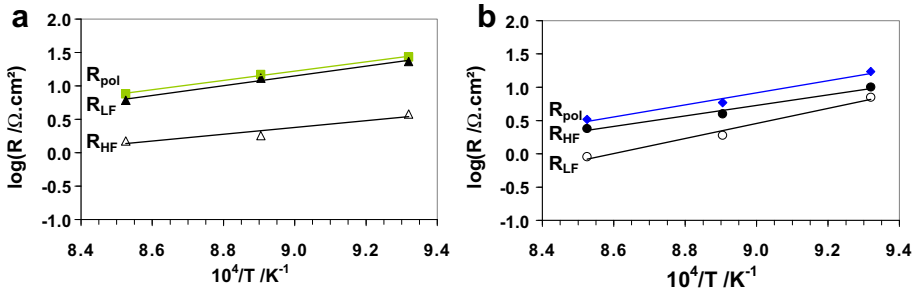

Fig. 6. Arrhenius diagrams of resistances for (a) LSCM and (b) LBCM electrodes at OCP in H_2–3% H_2O.

35% of the polarization resistance. An increase of the activation energies is also recorded (Table 4).

At this stage, it is worth mentioning that scattering on electrical parameters deduced from impedance diagrams has been determined for two pin-shaped LSCM electrodes (not shown here). Within the experimental accuracy, a variation by a factor of 2 of a resistance can be regarded as significant [61]. Although conductivities of LSCM and LBCM are similar in wet H_2 above 700 °C (Fig. 4), the recorded variation of R_{pol} does not originate from a modified current collecting within the anode. Accordingly, the lower polarization resistance of LBCM demonstrates that barium is effective in enhancing the oxidation rate of hydrogen.

A peculiar impedance parameter is the apex frequency which represents an identification signature of a described phenomenon since it does not depend on geometric dimensions of the measuring cell [62]. From the results of Fig. 7, one can infer that the origin of each specific impedance response is similar in both electrodes.

Between 800 and 900 °C, the capacitance of the HF contribution is about 8–20 μF cm^{-2} for LBCM and is 15–20 μF cm^{-2} for LSCM. Regardless of the composition, this capacitance is essentially independent of the measuring temperature. These values agree well with those generally reported for an interfacial process [63,64]. For instance, at 1000 °C in wet H_2, the capacitance of the high frequency response for a nickel electrode is around 50 μF cm^{-2} and around 100 μF cm^{-2} for Ni–YSZ cermet electrodes [64]. In addition, the HF resistance is nearly insensitive to the gas composition (Fig. 8) and the activation energy is rather close to those reported for the high frequency contribution evidenced respectively at 800 and 900 °C for a $La_{0.75}Sr_{0.25}Cr_{0.5}Mn_{0.5}O_3$–YSZ composite anode (1.49 eV) [45] and between 710 and 910 °C for a $La_{0.4}Sr_{0.6}Ti_{1-x}Mn_xO_3$/YSZ interface (0.9–1.5 eV) [65]. At this stage, the HF response can be attributed to the transfer of ionic species at the anode/YSZ interface [66,67]. The capacitance of the LF process was 0.2 mF cm^{-2} for LSCM and is 0.3–0.6 mF cm^{-2} for LBCM. The capacitance corresponding to adsorption of monocharged species on a Ni–YSZ electrode has been calculated to be of the order of

Table 4
Activation energies of elementary contributions and total polarization resistance in H_2–3% H_2O.

	LSCM	LBCM
$E_a(R_{HF})$ eV	1.02	1.58
$E_a(R_{LF})$ eV	1.45	2.27
$E_a(R_{pol})$ eV	1.38	1.82

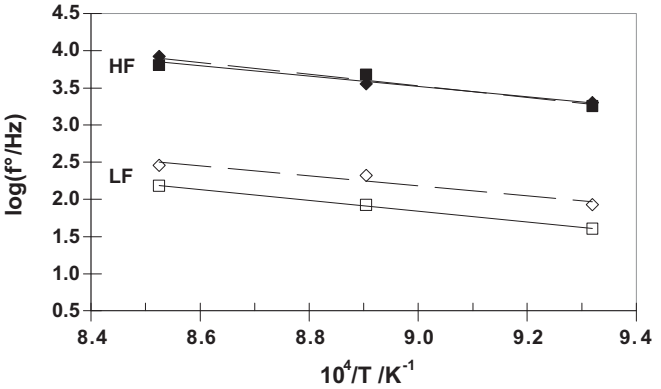

Fig. 7. Arrhenius diagram of apex frequencies for electrodes LSCM (□) and LBCM (◇) at OCP in H_2–3% H_2O.

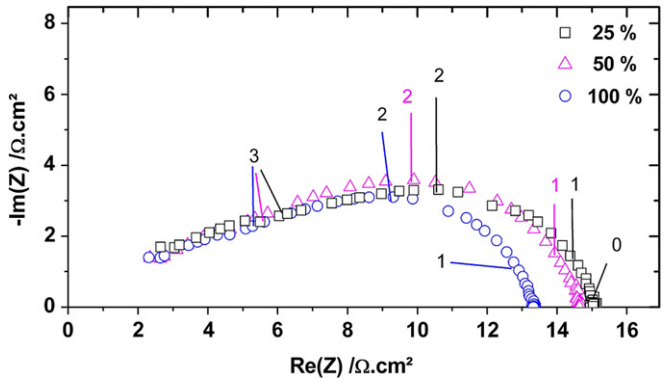

Fig. 8. Electrode characteristics of LBCM as a function of hydrogen concentration (expressed in %) recorded at OCP in Ar–H_2–3% H_2O at 800 °C.

10 mF cm^{-2} [68]. At 1000 °C in wet H_2, the capacitance of the low frequency response of a Ni electrode is around 1 mF cm^{-2} [63]. Since the LF contribution depends on the hydrogen concentration in humidified H_2 (Fig. 8), it is proposed to be related to an adsorption step [56,65,69]. Indeed, a surface diffusion process is unlikely since the corresponding activation is expected to be lower [70]. For LSCM, the activation energy is in agreement with literature data varying between 1.3 and 1.7 eV [45,65]. The higher value determined for LBCM is rather close to that of oxygen diffusion in LSM [71]. The contribution of bulk transport to the oxidation reaction can be taken into account since the use of dense electrodes necessarily couples bulk transport and surface reaction [58].

The results in OCP conditions indicate that barium substitution enhances the kinetics of hydrogen oxidation. The superior performance of LBCM is also demonstrated by its polarization performance (Fig. 9). No limiting current density is evidenced in the chosen experimental conditions. At an overpotential of 0.4 V, the current density is 0.02 and 0.71 A cm^{-2} for the oxidation of hydrogen on LSCM and LBCM at 800 °C, respectively. For the LBCM anode, the overpotential is even lower than for porous LSCM electrodes [34,72]. For instance, the current density is below 0.4 A cm^{-2} for a LSCM–YSZ composite anode in 97% H_2–3% H_2O at 800 °C [44]. In agreement with the shape of steady state curves, the polarization resistance decreases with increasing anode overpotential for both electrodes (Fig. 10), as already observed for porous perovskite based anodes [2,58]. At 850 °C, R_{pol} decreases by a factor of 3.5–3.7 between OCP and 0.4 V. The decrease of R_{pol} is mainly due to that of the HF resistance for LBCM (not shown here). Applying a positive potential results in an increase of the effective oxygen partial pressure causing an increase of total (mainly electronic) conductivity of LBCM electrode (Fig. 4). One could thus suggest a contribution of current collection at the electrode/platinum interface in the HF response. But the decrease of R_{pol} of the LSCM anode with overpotential mostly originates from the LF contribution while the HF resistance remains nearly constant. This further indicates that the HF process is mainly related to an ionic transfer at the electrode/YSZ interface.

The electrocatalytic properties of perovskite oxides depend on the nature of B-site cations [2,58] but are not only governed by these sites [73]. Manganese ions can be expected to be the most redox active sites in reducing conditions [74]. Hydrogen adsorbed on the electrode surface is oxidized through reduction of the B-site cations. For low oxygen partial pressures, these surface reaction sites are then re-oxidized by lattice oxygen diffusing from the electrode/YSZ interface to the electrode surface [54], suggesting that bulk ion transport can play a significant role on the oxidation kinetics of hydrogen. The mobility of oxygen ions through the oxide depends on the electronegativity difference between cations and anions [74]. For instance, the substitution of manganese by chromium in $Sr_{0.7}Ce_{0.3}Mn_{0.9}Cr_{0.1}O_3$ corresponds to a decrease of this difference and yields a higher oxygen permeability flux despite a lower oxygen nonstoichiometry [67]. Since the manganese content is constant, oxidation kinetics can be modified by the nature of cations substituted in A-sites, assuming that chromium oxidation state remains to +3 [75]. Substitution of strontium ($\chi = 0.95$) by barium ($\chi = 0.89$) results in an increase of the electronegativity difference between cationic sites (lanthanum $\chi = 1.10$) and anionic sites ($\chi = 3.44$). This yields an increase in

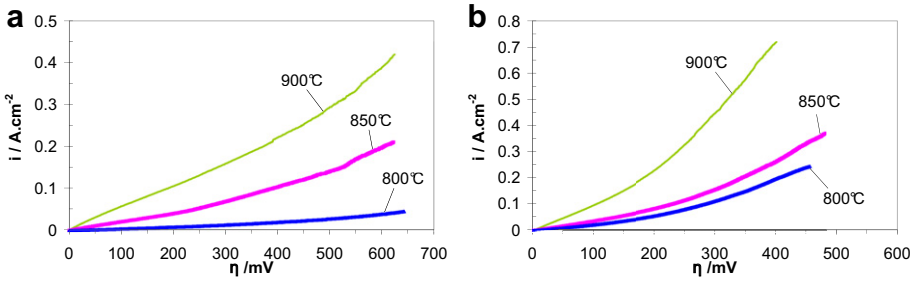

Fig. 9. Steady state polarization curves recorded on (a) LSCM and (b) LBCM in H_2–3% H_2O.

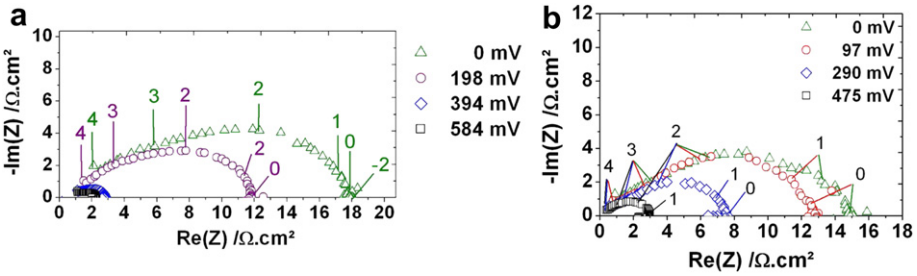

Fig. 10. Electrode characteristics recorded in H_2–3% H_2O on (a) LSCM at 850 °C and (b) LBCM electrodes at 800 °C for different overpotentials.

binding energy between cations and anions and a decrease in oxide ions mobility. Thus, oxidation kinetics on LBCM should be lower which is in contradiction with reported results (Fig. 9). However, the decrease in average electronegativity of cationic sites could also results in an increase in negative partial charge of anionic sites that would make active sites more basic, and thus favouring oxygen exchange to adsorbed species on the surface of the electrode material. As the current increases, the non-linear decrease of the polarization resistance could result from an improved oxygen anion flux due to increased oxygen stoichiometry [58]. The variation of the LF resistance is in agreement with this assumption.

4. Conclusions

Single phase barium-doped lanthanum chromo-manganite $La_{0.75}Ba_xSr_{0.25-x}Cr_{0.5}Mn_{0.5}O_3$ with $x = 0.1$ and 0.25 materials were synthesized in neutral atmosphere. The rhombohedral crystal structure of strontium-doped lanthanum chromo-manganite (LSCM) is not modified by barium substitution. LSCM and barium substituted LSCM materials are stable both in air and in wet reducing environment, and the stability is improved by barium substitution in dry reducing environment compared to LSCM. In argon and wet hydrogen, a p-type conduction behaviour has been evidenced and the total conductivity decreases with the oxygen partial pressure. Whereas electrical conductivity increases with barium content till reaching 26 S cm^{-1} at 900 °C in argon, it decreases with barium substitution in wet hydrogen (0.5 S cm^{-1} at 900 °C for $x = 0.1$ and 0.25). LBCM ($x = 0.25$) shows a better electrochemical activity for the hydrogen oxidation reaction, as compared to LSCM. The anodic performance of LBCM suggests that it represents a potential candidate for an SOFC anode material. These properties depend on the oxygen ions supply to active reaction sites. The mechanism of hydrogen oxidation is considered to involve two main steps: an ionic transfer at the anode/electrolyte interface and an adsorption step at the electrode surface. Since this material shows a high stability either in wet and dry environments, it would be interesting to perform electrochemical tests in methane or CO_2 containing atmosphere and/or in solid oxide electrolyser cell cathode operating conditions, what will be the object of a forthcoming study.

References

[1] A. Atkinson, S. Barnett, R.J. Gorte, J.T.S. Irvine, A.J. McEvoy, M. Mogensen, S.C. Singhal, J. Vohs, Nat. Mater. 3 (2004) 17–27.
[2] S. Tao, J.T.S. Irvine, J. Electrochem. Soc. 151 (2004) A252–A259.
[3] J. Canales-Vásquez, S.W. Tao, J.T.S. Irvine, Solid State Ionics 159 (2003) 159–165.
[4] S.M. Plint, P.A. Connor, S. Tao, J.T.S. Irvine, Solid State Ionics 177 (2006) 2005–2008.
[5] E.S. Raj, J.A. Kilner, J.T.S. Irvine, Solid State Ionics 177 (2006) 1747–1752.
[6] L. Wang, R. Merkle, J. Maier, T. Acartürk, U. Starke, Appl. Phys. Lett. 94 (2009) 0719081–0719083.
[7] J. Pena-Martinez, D. Marrero-Lopez, J.C. Ruiz-Morales, C. Savaniu, P. Nunez, J.T.S. Irvine, Chem. Mater. 18 (2006) 1001–1006.
[8] G. Kim, G. Corre, J.T.S. Irvine, J.M. Vohs, R.J. Gorte, Electrochem. Solid-State Lett. 11 (2008) B16–B19.
[9] X.J. Chen, Q.L. Liu, K.A. Khor, S.H. Chan, J. Power Sources 165 (2007) 34–40.
[10] X. Zhu, Z. Lü, B. Wei, Y. Zhang, M. Liu, X. Huang, W. Su, J. Electrochem. Soc. 157 (2010) B691–B696.
[11] S. Barison, M. Fabrizio, C. Mortalo, P.L. Antonucci, V. Modafferi, R. Gerbasi, Solid State Ionics 181 (2010) 285–291.
[12] M. van den Bossche, S. McIntosh, J. Catal. 255 (2008) 313–323.
[13] N. Danilovic, A. Vincent, J.-L. Luo, K.T. Chuang, R. Hui, A.R. Sanger, Chem. Mater. 22 (2010) 957–965.
[14] M. van den Bossche, S. McIntosh, Chem. Mater. 22 (2010) 5856–5865.
[15] F.C. Fonseca, E.N.S. Mucillo, R. Mucillo, D.Z. de Florio, J. Electrochem. Soc. 155 (2008) B483–B487.
[16] X. Chen, W. Ma, J. Yu, Adv. Mater. Res. 79-82 (2009) 123–126.
[17] E. Lay, G. Gauthier, S. Rosini, C. Savaniu, J.T.S. Irvine, Solid State Ionics 179 (2008) 1562–1566.
[18] S. Raz, K. Sasaki, J. Maier, I. Riess, Solid State Ionics 143 (2001) 181–204.
[19] T. Horiuchi, K. Sakuma, T. Fukui, Y. Kubo, T. Osaki, T. Mori, Appl. Catal. A Gen. 144 (1996) 111–120.
[20] G.S. Gallego, F. Mondragón, J. Barrault, J.-M. Tatibouët, C. Batiot-Dupeyrat, Appl. Catal. A Gen. 311 (2006) 164–171.
[21] J.R. Mawdsley, T.R. Krause, Appl. Catal. A Gen. 334 (2008) 311–320.
[22] J. Yi, M. Schroeder, T. Weirich, J. Mayer, Chem. Mater. 22 (2010) 6246–6253.
[23] A. Waindich, A. Möbius, M. Müller, J. Membr. Sci. 337 (2009) 182–187.
[24] L. Yang, Y. Choi, W. Qin, H. Chen, K. Blinn, M. Liu, P. Liu, J. Bai, T.A. Tyson, M. Liu, Nat. Commun. 1359 (2011) 1–9.
[25] L. Zhang, X. Chen, S.P. Jiang, H.Q. He, Y. Xiang, Solid State Ionics 180 (2009) 1076–1082.
[26] M.S.G. Baythoun, F.R. Sale, J. Mater. Sci. 17 (1982) 2757–2769.
[27] E. Lay, G. Gauthier, L. Dessemond, Solid State Ionics 189 (2011) 91–99.
[28] J. Rodriguez-Carjaval, Physica B 192 (1993) 55–69.
[29] J.F. Bérar, P. Lelann, J. Appl. Cryst. 24 (1991) 1–5.
[30] M. Zahid, I. Arul Raj, F. Tietz, P. Lersch, D. Stöver, in: S.C. Singhal, J. Mizusaki (Eds.), Proc. 9th Int. Symp, Solid Oxide Fuel Cells (SOFC-IX), vol. 2, The Electrochemical Society, Pennington, NJ, 2005, pp. 1708–1716.
[31] R.D. Shannon, C.T. Prewitt, Acta Crystallogr. B25 (1996) 925–946.
[32] L.A. Al-Hajji, M.A. Hasan, M.I. Zaki, Thermochim. Acta 483 (2009) 8–14.
[33] M. Al Daroukh, V.V.V. ashook, H. Ullmann, F. Tietz, I. Arual Raj, Solid State Ionics 158 (2003) 141–150.
[34] V.V. Kharton, E.V. Tsipis, I.P. Marozau, A.P. Viskup, J.R. Frade, J.T.S. Irvine, Solid State Ionics 178 (2007) 101–103.
[35] O. Peña, M. Bahout, D. Gutierrez, P. Duran, C. Moure, Solid State Sci. 5 (2003) 1217–1227.
[36] G.V. Subba Rao, B.M. Wanklyn, C.N.R. Rao, J. Phys. Chem. Solids 32 (1971) 345–358.
[37] J.B. Goodenough, J. Appl. Phys. 37 (1966) 1415–1422.
[38] G.Ch. Kostogloudis, N. Vasilakos, Ch. Ftikos, Solid State Ionics 106 (1998) 207–218.
[39] F. Tietz, F.J. Dias, D. Simwonis, D. Stöver, J. Eur. Ceram. Soc. 20 (2000) 1023–1034.
[40] M.D. Gross, J.M. Vohs, R.J. Gorte, Electrochem. Solid-State Lett. 10 (2007) B65–B69.
[41] J. Newman, J. Electrochem. Soc. 113 (1966) 501–502.
[42] Z.H. Bi, J.H. Zhu, J. Electrochem. Soc. 158 (2011) B605–B613.
[43] L. Deleebeeck, J.L. Fournier, V. Birss, Solid State Ionics 181 (2010) 1229–1237.
[44] S.P. Jiang, X.J. Chen, S.H. Chan, J.T. Kwok, J. Electrochem. Soc. 153 (2006) A850–A856.
[45] S.P. Jiang, X.J. Chen, S.H. Chan, J.T. Kwok, K.A. Khor, Solid State Ionics 177 (2006) 149–157.
[46] J.C. Ruiz-Morales, J. Canales-Vasquez, J. Pena-Martinez, D. Marrero-Lopez, P. Nunez, Electrochim. Acta 52 (2006) 278–284.
[47] X.J. Chen, Q.L. Liu, S.H. Chan, N.P. Brandon, K.A. Khor, J. Electrochem. Soc. 154 (2007) B1206–B1210.
[48] J. Pena-Martinez, D. Marrero-Lopez, J.C. Ruiz-Morales, B.E. Buergler, P. Nunez, L.J. Gauckler, J. Power Sources 159 (2006) 914–921.
[49] S. Zha, P. Tsang, Z. Cheng, M. Liu, J. Solid State Chem. 178 (2005) 1844–1850.
[50] C. Jin, C. Yang, F. Chen, J. Electrochem. Soc. 158 (2011) B1217–B1223.
[51] S. McIntosh, J.M. Vohs, R.J. Gorte, Electrochem. Solid-State Lett. 11 (2003) A240–A243.
[52] S. Park, J.M. Vohs, R.J. Gorte, Nature 404 (2000) 265–267.
[53] S. Tao, J.T.S. Irvine, J. Electrochem. Soc. 151 (2004) A497–A503.
[54] J. Wan, J.H. Zhu, J.B. Goodenough, Solid State Ionics 177 (2006) 1211–1217.
[55] G. Kim, S. Lee, J.Y. Shin, G. Corre, J.T.S. Irvine, J.M. Vohs, R.J. Gorte, Electrochem. Solid-State Lett. 12 (2009) B48–B52.
[56] S. Primdhal, M. Mogensen, Solid State Ionics 152-153 (2002) 597–608.
[57] H.J.M. Bouwmeester, H. Kruidhof, A.J. Burggraaf, Solid State Ionics 72 (1994) 185–194.
[58] M. van den Bossche, R. Matthews, A. Lichtenberg, S. McIntosh, J. Electrochem. Soc. 157 (2010) B392–B399.
[59] S. Tao, J.T.S. Irvine, J.A. Kilner, Adv. Mater. 17 (2005) 1734–1737.
[60] S. Primdhal, J.R. Hansen, L. Grahl-Madsen, P.H. Larsen, J. Electrochem. Soc. 148 (2001) A646–A651.
[61] E. Lay, Ph.D, Grenoble, France, 2009.
[62] E. Schouler, Ph.D, Grenoble, France, 1979.
[63] S.P. Jiang, S.P.S. Badwal, Solid State Ionics 123 (1999) 209–224.
[64] P. Holtappels, L.C. Vinke, L.G.J. de Haart, U. Stimming, J. Electrochem. Soc. 146 (1999) 2976–2982.
[65] Q.X. Fu, F. Tietz, D. Stöver, J. Electrochem. Soc. 153 (2006) D74–D83.
[66] S.W. Tao, J.T.S. Irvine, S.M. Plint, J. Phys. Chem. B 110 (2006) 21771–21776.
[67] A.A. Yaremchenko, A.V. Kovalevsky, V.V. Kharton, Solid State Ionics 179 (2008) 2181–2191.
[68] S. Primdhal, M. Mogensen, J. Electrochem. Soc. 144 (1997) 3409–3419.
[69] P. Blennow, K.K. Hansen, L.R. Wallenberg, M. Mogensen, Solid State Ionics 180 (2009) 63–70.
[70] M. Vogler, A. Bieberle-Hütter, L. Gauckler, J. Warnatz, W.G. Bessler, J. Electrochem. Soc. 156 (2009) B663–B672.
[71] D. Kek, M. Mogensen, S. Pejovnik, J. Electrochem. Soc. 148 (2001) A878–A886.
[72] X.C. Lu, J.-H. Zhu, Solid State Ionics 178 (2007) 1467–1475.
[73] N. Yamazoe, Y. Teraoka, Catal. Today 8 (1990) 175–182.
[74] B. Levasseur, S. Kaliaguine, Appl. Catal. B Env. 88 (2009) 305–314.
[75] M. Oishi, K. Yashiro, K. Sato, J. Mizusaki, T. Kawada, J. Solid State Chem. 181 (2008) 3177–3184.